Computers and Concrete, *Vol. 24, No. 2 (2019) 173-183*
DOI: https://doi.org/10.12989/cac.2019.24.2.173

Interface slip of post-tensioned concrete beams with stage construction: Experimental and FE study

Hin Foo Low[1a], Sih Ying Kong[*1], Daniel Kong[1b] and Suvash Chandra Paul[1,2c]

[1]*School of Engineering, Monash University Malaysia, Bandar Sunway, 47500, Malaysia*
[2]*Department of Civil Engineering, International University of Business Agriculture and Technology, Dhaka 1230, Bangladesh*

(Received March 15, 2019, Revised June 14, 2019, Accepted June 20, 2019)

Abstract. This study presents experimental and numerical results of prestressed concrete composite beams with different casting and stressing sequence. The beams were tested under three-point bending and it was found that prestressed concrete composite beams could not achieve monolith behavior due to interface slippage between two layers. The initial stress distribution due to different construction sequence has little effect on the maximum load of composite beams. The multi-step FE analyses could simulate different casting and stressing sequence thus correctly capturing the initial stress distribution induced by staged construction. Three contact algorithms were considered for interaction between concrete layers in the FE models namely tie constraint, cohesive contact and surface-to-surface contact. It was found that both cohesive contact and surface-to-surface contact could simulate the interface slip even though each algorithm considers different shear transfer mechanism. The use of surface-to-surface contact for beams with more than 2 layers of concrete is not recommended as it underestimates the maximum load in this study.

Keywords: prestressed concrete beam; finite element (FE) analysis; interface shear; post-tensioning; interface slip; staged construction

1. Introduction

Concrete composite structures are produced by casting a layer of concrete on top of precast concrete elements or strengthening of existing concrete structural elements using concrete overlay. Sufficient interface shear strength is important for concrete composite structures to achieve monolithic behavior. The interface shear strength is governed by concrete adhesion, friction interaction and reinforcement crossing the interface. Extensive experimental investigations have been conducted to study the interface shear of concrete composite structures.

Patnaik (2001) studied behavior of composite rectangular and T beams with smooth interface. Slippage at the interface was observed and the beams could not achieve monolithic behavior. The concrete compressive strength had no effects on the horizontal shear strength of composite beams with smooth interface. Loov and Patnaik (1994) showed that the rough interface prepared by coarse aggregates protruding from the surface but firmly fixed in the matrix could develop adequate shear resistance for concrete composite beams.

The stress in the stirrups crossing the interface only increased when the interface shear stress exceeded 1.5 MPa. The "push-off" experimental results on different surface textures by Mohamad *et al*. (2015) revealed that the mean peak height has the most significant effect on the pre-crack interface shear strength. An experimental study was performed by Halicka (2011) to study composite beams with three interface configurations namely (i) with chemical bonding of concrete alone, (ii) with shear reinforcement only and (iii) with both chemical bonding of concrete and shear reinforcement. The beams with both chemical bonding of concrete and shear reinforcement sustained the highest average maximum load, while the beams with shear reinforcement only demonstrated the lowest average maximum load. He *et al*. (2017) investigated influence of interface roughness and adhesion agents on new-to-old concrete bond. The interface adhesion agents improved bond strength at the interface, the efficiency varied for different types of adhesion. These research indicated that the interface shear strength increased with increased surface roughness and shear reinforcement crossing the interface should be provided to complement chemical bonding of concrete in order to achieve the monolith behaviors for concrete beams.

Effects of interface shear strength on the structural response of composite hollow core slabs have been reported by several researchers. Adawi *et al*. (2015) carried out a comprehensive experimental program to evaluate the interface performance of composite hollow-core slab with machine-cast finish and concrete topping through a series of pull-off, push-off and full-scale bending tests. The results

∗Corresponding author, Ph.D.
E-mail: kong.sih.ying@monash.edu
[a]Ph.D. Student
E-mail: low.hin.foo@monash.edu
[b]Ph.D.
E-mail: Daniel.kong@monash.edu
[c]Ph.D.
E-mail: suvash.chandra@monash.edu

http://www.techno-press.org/?journal=cac&subpage=8
ISSN: 1598-8198 (Print), 1598-818X (Online)

indicated that hollow-core slabs with machine-cast surfaces could be considered to act compositely with the concrete topping. Roughened interfaces developed higher shear strength and horizontal slip capacity than machine-finished interfaces (Mones and Breña 2013). The flexural test results of precast concrete hollow-core slabs with cast-in-place concrete topping showed that composite action increased flexural stiffness and cracking load (Baran 2015). Interface slip occurred before the full potential flexural strength of composite sections could be achieved. Most of research only focused on the effects of surface roughness for interface shear transfer of composite slabs, and machine cast surfaces showed lower interface shear strength than roughened surfaces.

Research findings showed that the interface shear between lightweight concrete-normal weight concrete composite structures could be different from the normal weight concrete composite structures. Fang *et al*. (2018) conducted flexural tests to evaluate interface shear behavior of composite T beams fabricated using normal weight concrete beam and lightweight concrete slab. Shear reinforcement was provided across the beam and slab interface. It was found that AASHTO and ACI design codes underestimated the interface shear capacities of these beams and a new empirical equation was proposed based on the experimental results available in the literature. The push-off test results by Lesley *et al*. (2016) revealed that granular size of lightweight coarse aggregate has little effect on the interface shear strength. The ultimate shear stress of push-off samples with a roughened interface was affected by type of lightweight aggregates, while it has no effects on the samples with smooth interface. Concrete composites with lightweight concrete slabs demonstrated higher interface shear strength compared to normal weight concrete slab specimens at the same concrete strength as reported by Jiang *et al*. (2016). Costa *et al*. (2018) studied the bond strength of lightweight aggregate concrete (LWAC) to normal density concrete and LWAC-to-LWAC interfaces through slant shear and splitting tests. For smooth interface, the interface strength was influenced by the binding matrix strength of concrete overlay. The lightweight aggregates properties were important for rougher surface. The experimental results of samples with rough interfaces were higher than the predicted results by Eurocode 2 and fib Model code 2010. Most of the research results suggested the existing codes underestimated the interface shear strength of lightweight concrete composite structures.

Strengthening existing concrete structures with a new concrete layer is an economical and effective technique. Sufficient interface shear strength should be provided to achieve monolithic behavior. Seible and Latham (1990) showed that reinforcement dowels in the horizontal construction joints only become effective after large interface displacement occurred. It was found that the minimum interface shear reinforcement ratio of 0.2% specified by Model code 1978 was realistic to ensure monolithic behavior of concrete composites. Julio *et al*. (2010) found that the shear strength of interfaces with low reinforcing ratios corresponded to the de-bonding stress of concrete. While the shear strength was reached after a critical slip for interface with higher reinforcing ratios. Results from both research showed that shear reinforcement contributed to interface shear transfer only after the slip occurred at the interface due to failure of cohesion of concrete. Tsioulou *et al*. (2013) studied effectiveness of strengthening concrete beams by adding an additional concrete layer on top and at the soffit of existing concrete beams. It was found that placing the additional concrete layer at the tensile side (soffit) required very good roughened surface in order to achieve the capacity of full composite action. By placing the additional layer of concrete at the compression side (top), only negligible slippage was observed. Sufficient amount of reinforcement crossing the interface should be provided for RC slabs strengthened by reinforced concrete overlay on the tensile face. Experimental results showed that the maximum load increased by up to three times for samples with properly anchored rebar crossing the interface compared to samples without reinforcement (Fernades *et al*. 2017). Yin *et al*. (2017) observed de-bonding between ultra-high performance concrete overlays and the slabs as no reinforcement was provided crossing the interface.

Numerical study of concrete composite structures is challenging due to complex interaction at the interface. Inclusion of bond-slip behavior at the interface is important to correctly simulate the response of concrete composites. Kwak *et al*. (2006) proposed tendon models which by modifying the stress-strain relationships of tendon, the tendon-concrete interaction effects could be considered. These tendon models simplified the nonlinear finite element analysis of PSC structures with bonded and unbonded tendons as the proposed models do not require a double node to simulate tension stiffening or slip at the interface. These concepts have been adopted to predict the response of steel-concrete composite and concrete composite beams with partially composite action (Kwak and Hwang 2010). Validation of FE models against the experimental results showed that the proposed formulation could accurately predict the response of steel-concrete composite and concrete composite beams with partially composite action. Two dimensional FE models were developed and validated against the experimental results of push-off tests to study interfacial behavior of composite concrete members (Costa *et al*. 2012). The concrete interface was modelled using zero-thickness interface linear elements which ignored the failure at the interface. A parametric study was performed to investigate effects of elastic shear stiffness, interface friction angle, dilatancy angle, cohesion, fracture energy and bond slip between steel and concrete. The numerical study demonstrated that concrete damage plasticity material model was capable of predicting the response of partial depth precast prestressed concrete bridge decks with cast in situ concrete topping (Ren *et al*. 2015). Adawi *et al*. (2016) presented a realistic finite element modelling technique to simulate the staged construction of precast hollow-core slabs and additional topping concrete layers. The interaction at interface of the composite hollow-core slab was modelled using nonlinear spring elements in both tangential and normal direction, while the staged construction was simulated by changing the stiffness of concrete topping

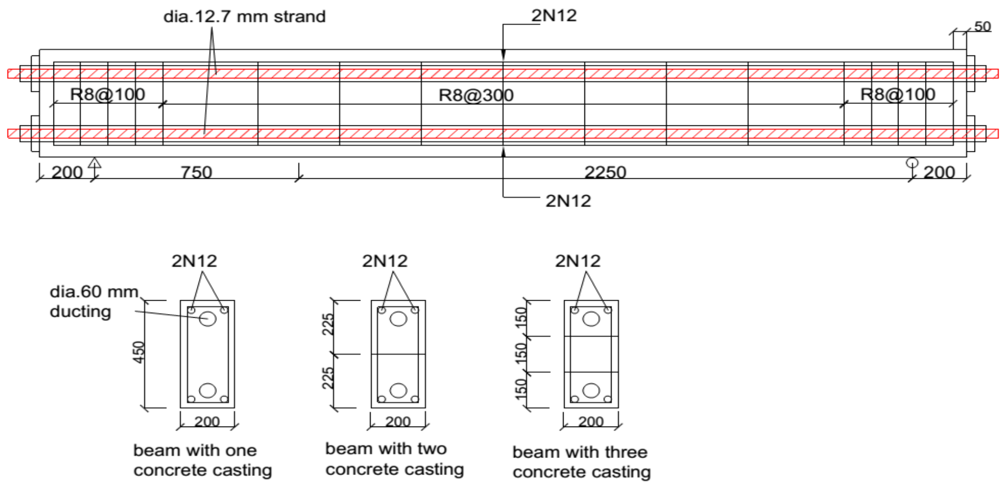

Fig. 1 Details of post-tensioned concrete beams. (all dimensions in mm)

Table 1 Maximum load, stiffness and ductility of prestressed concrete composite beams with different construction sequence

	Maximum load							Elastic stiffness (kNm^2) $\times 10^3$	Ductility factor
	Exp. (kN)	FE mon-olithic or tie (kN)	FE cohesive (kN)	FE fric. (kN)	FE tie/ Exp.	FE cohesive/Exp.	FE fric. /Exp.		
Control 1	221.4	210.8	-	-	0.95	-	-	6.06	4.7
Control 2	220.3				0.96	-	-	5.95	4.4
2C1S 1	216.4	208.7	186.7	192.9	0.96	0.86	0.89	6.18	4.2
2C1S 2	213.3				0.98	0.88	0.90	6.18	3.6
2C2S 1	207.0	203.8	184.5	185.4	0.98	0.89	0.90	5.42	3.3
2C2S 2	200.6				1.02	0.92	0.92	6.10	4.9
3C2S 1	207.3	210.5	193.9	153.3	1.02	0.94	0.74	5.73	4.5
3C2S 2	198.1				1.06	0.98	0.77	5.98	4.6

during the analysis.

It was found that very limited research has been conducted to study the interface slip effects on the response of prestressed concrete composite beams prepared using staged construction technique considering different casting and stressing sequence. Staged construction is typically adopted for construction of prestressed transfer structures due to their enormous thickness. The thickness could be up to 2-3 m in order to support buildings with more than 20 storeys height. To reduce the load sustained by the temporary formworks, concrete is poured up to three layers depending on the thickness of transfer structures and site conditions. Once concrete has hardened and prestressing force has been applied, the first concrete layer sustains the weight of the casting of second and third layers reducing the load transferred to formworks. In this study, three-point bending test was conducted to evaluate static response of post-tensioned concrete composite beams with various casting and stressing sequence. The results presented in this study may be useful for the analysis of prestressed transfer structures. It was found that the interface slip reduced maximum load of concrete composite beams. The multi-step FE analyses developed in this study could correctly predict the initial stress distribution in the beams caused by different casting and stressing sequence. Three contact algorithms evaluated were tie constraint, cohesive contact and surface-to-surface contact. It was found that tie constraint and cohesive contact predicted flexural stiffness more accurately than the surface-to-surface contact. Both cohesive contact and surface-to-surface contact considered interface slip and predicted the maximum load accurately. However the surface-to-surface contact was only suitable for composite beams with two layers of concrete.

2. Preparation and flexural testing of post-tensioned concrete composite beams

Fig. 1 shows the geometry and reinforcement details of post-tensioned concrete beams. The beam was 3.4 m in length and 12 mm diameter bars were provided as top and bottom flexural reinforcements. The 12 mm diameter bars were used as flexural reinforcement so that ductile failure could be achieved at the maximum load about 200 kN. Shear links of 8 mm diameter and 100 mm spacing were provided at both ends to minimize the risk of concrete cracking during stressing.

The shear links were placed at 300 mm spacing for the rest of the beam. Two 12 mm diameter U-shaped bars were provided at each end to prevent bursting and spalling of concrete near the anchorage zone. One straight metal duct was placed at a distance of 150 mm below the beam centre and another one at the same distance above the beam centre before concrete casting. Ideally, the pretsressing strands

Fig. 2 Experimental setup for three-point bending test at the quarter span

should adopt parabolic profile where the strands should be placed at the tensile zone of beams. For staged construction of continuous beams, the strands are placed near to the top of concrete beam over the column supports then extended to the bottom at mid-span by adopting parabolic profile. The parabolic profile could not be achieved in this study due to the limitation of beam dimensions prepared in this study. To simulate the staged casting and sequence stressing construction process, the straight strands were placed in each concrete layer in this study. Once concrete has achieved sufficient strength after 14 days, the 12.7 mm diameter strands were stressed to 75% of its ultimate tensile strength (1861 MPa) to apply prestressing force to the concrete beams. The prestressing strands were held in place by an anchorage system that consisted of the anchor grips and anchor plates. Grout was pumped into both metal ducts after stressing to ensure proper bonding between concrete beam and strands.

Four sets of specimens were prepared by varying number of concrete casting and stressing sequence to investigate effects of stress distribution and concrete joints on the static response of post-tensioned concrete beams. The casting and stressing sequence for all beams are presented in Table 1. Two beams were prepared for each set of specimen. Ready mix concrete was used for beams preparation and it is important to note that the surface finishes at the interface could be considered as rough surface because the coarse aggregates were protruding from the surface after casting. Concrete cylinders were prepared and cured at ambient temperature until the day of concrete composite beams testing. The average compressive strength for six cylinders from first and second batches of concrete was 35.06 MPa with a coefficient of variation of 4.46%.

Fig. 2 illustrates three-point bending test setup at the quarter span to assess the bending behaviour of the post-tensioned beams. Three-point bending at quarter span was chosen with the intention to ensure large interface slip occurred at the shorter side of beams due to lower shear resistance from concrete bonding. The distance between supports was 3000 mm. Two steel cylinders were placed at the quarter span from one of the supports to load the beams at a constant displacement rate of 0.05mm/s. The load and displacement of beams were recorded using a data logger until the beams failed

3. Experimental result

Fig. 3 shows the load-displacement curves for all the

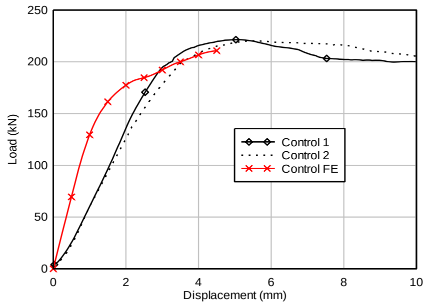

(a) control beams

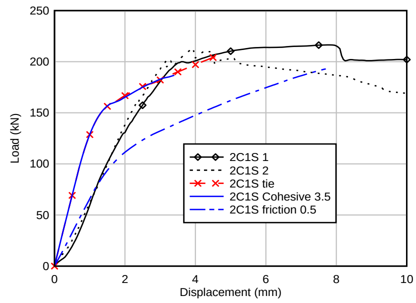

(b) two casts and simultaneous stressing (2C1S) beams

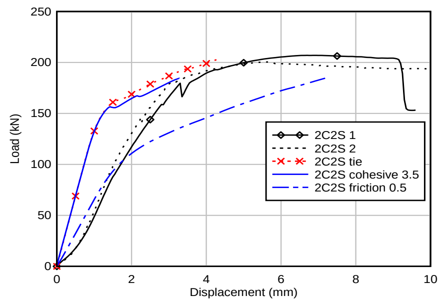

(c) two casts and sequenced stressing (2C2S) beams

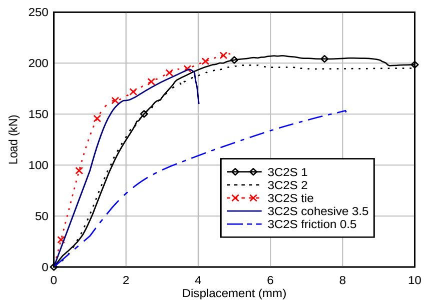

(d) three casts and sequenced stressing (3C2S) beams

Fig. 3 Load vs displacement at quarter span for beams with different casting and stressing sequence

beams. The initial stiffness of beams was presented in Table 2. The initial stiffness was similar for all the beams except 2C1S 1, which was about 10% lower than the average stiffness. This discrepancy could be due to the experimental error, as the staged construction should have no effect on the beam stiffness before crack initiation. The hairline flexural crack was first observed at the soffit of loaded quarter span with the load ranged from 115 kN to 135 kN for all the beams and it has negligible effect on the flexural stiffness of all the beams. As the load further increased, the initial flexural crack propagated upward and the crack width

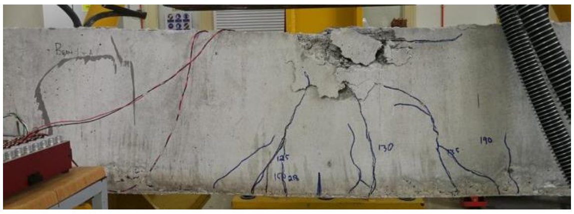

(a) tensile cracking and compression crushing of the control beam

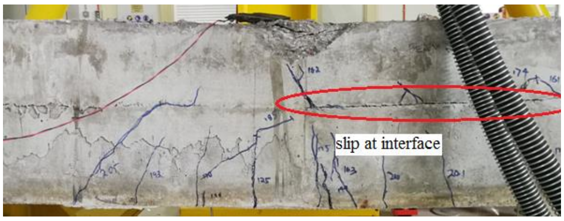

(b) tensile cracking, interface slip and compression crushing of the 2C1S beam

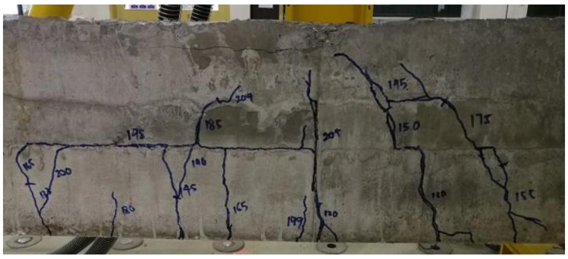

(c) tensile cracking, interface slip and compression crushing of the 3C2S beam

Fig. 4 Experimental observed damage on beams at the loaded quarter span

increased. In the meantime, new cracks formed adjacent to the first crack. It is important to note that the crack propagation direction and distribution were affected by concrete casting sequence. For the control beams, the flexural cracks propagated upward and flexural shear cracks could be observed as shown in Fig. 4(a). The control beams demonstrated ductile behaviour with the maximum load of 221.4 kN and 220.3 kN, before the beams failed by concrete crushing underneath the loading point. For the beams with two and three concrete casting (2C1S, 2C2S and 3C2S), flexural cracks initiated in the similar pattern as the control beams. However, as cracks reached the interface of two layers of concrete, some cracks propagated along the interface before they continued diagonally into the next layer of concrete. The strength at the interface was lower than the concrete cast monolithically, resulting in the crack propagation at the interface. The crack propagation at the interface resulted in failure of adhesion (chemical bonding of concrete) and thereafter the interface shear was sustained by friction interaction between surfaces and dowel action by the stirrups. All the beams with staged casting demonstrated a lower stiffness after 180 kN compared to control beams due to interface slip. The 2C1S beams demonstrated similar crack distribution with the 2C2S beams as shown in Fig. 4(b). Fig. 4(c) shows severe concrete cracking at the interface between bottom layer and middle layer of the 3C2S beam. Minor cracking at the interface between middle layer and top layer of concrete could be observed. It could be observed that beams with staged casting showed more cracks compared to the control beams. Some cracks initiated at the soffit of the second concrete layer due to interface slip as shown in Fig. 4 (b) and (c). Similar results were reported by Fang *et al*. (2018). The maximum load achieved by beams with staged casting was lower than the control beams as tabulated in Table 2 due to the slip at the interface. The average reduction of maximum load for 2C1S, 2C2S and 3C2S beams was 2.7%, 7.7% and 8.2 %, respectively. These results demonstrated that the beams prepared in this study could not achieve monolithic behaviour due to the slip between concrete layers.

The discrepancy of maximum load reduction could be attributed to the small variations in the surface roughness at the interface which affected the interface shear strength. By comparing the results of 2C2S beams and 3C2S beams, the initial stress distribution due to different casting and stressing sequence seemed to have little effect on the maximum load capacity.

The theoretical maximum moment capacity for the control beam was determined using Eurocode 2 (Standardization 2005). The simplified concrete design stress block, yield stress of rebars and prestressing strand were used in the calculation of moment capacity. Materials and load factor were ignored. Eurocode predicted the maximum load of 197.3 kN, it underestimated the maximum load of the control beams 1 and 2 by 12.2% and 11.7%, respectively. The theoretical analysis underestimated the maximum load because the strain hardening effect of both prestressing strands and rebar was ignored in the analysis. The beams still demonstrated ductile response before they failed due to concrete crushing in the compression zone.

The ductility factor of the beams was presented in Table 2. The average ductility factor for control beams was about 4.6. For the beams with staged construction, two beams 2C1S 2 and 2C2S 1 showed lower ductility factor, below 4 while other beams demonstrated similar ductility with the control beams. More research is required to study effects of staged construction on the ductility of beams

Table 2 Concrete damage plasticity parameters used in the finite element analyses

Dilation angle, ψ	Eccentricity, ε	f_{bo}/f_{co}	K_c	Viscosity parameter
31	0.1	1.16	0.667	1×10^{-5}

4. Finite element analysis

The FE models developed in this study simulated different casting and stressing sequence of beams by defining multi-step analyses and these models could capture the stress distribution of concrete composite beams accurately. The interaction at the concrete interfaces was simulated using three contact algorithms and differences in the predicted behaviours were discussed.

4.1 Description of FE model

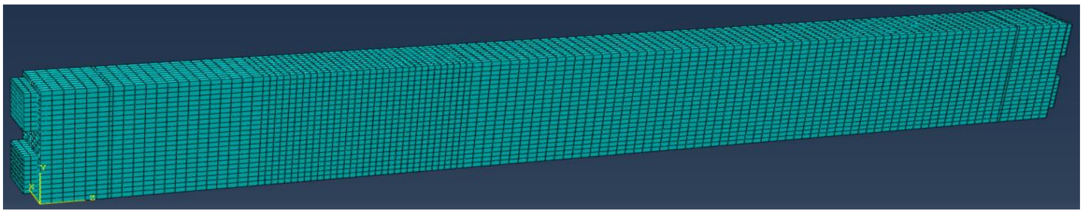

Fig. 5 Mesh discretization of FE model for post-tensioned concrete beam

All the beams were modelled in 3D using the commercial finite element program Abaqus/Standard. Abaqus static general analysis was used to analyze the response of beams considering material nonlinearity effects. The stiffness of beams was determined using incremental iterative method and full Newton method was employed to solve the nonlinear equilibrium equations. The whole beam was modelled in the analysis as the load was applied at the quarter-span. The concrete beam and end bearing plates were discretized using eight-node reduced integration continuum 3D solid elements (C3D8R). The end bearing plates were modelled in order to distribute the prestressing force from strands into concrete, avoiding unrealistic stress concentration. Kim and Kwak (2018) conducted a parametric study for bursting stress in the post-tensioned anchorage zone and proposed an improved design guideline by including influence of the duct hole.

Prestressing strands, rebar and shear links were modelled using 2-node beam elements. The loading cylinders and roller supports were omitted to simplify the analysis. The roller supports were replaced with the boundary condition defined over 10 mm width strip on the beam to avoid unrealistic local stress concentration. The vertical displacement at the support strips was restrained, while longitudinal and transverse displacements were unrestrained to simulate the roller supports. The loading was applied through prescribed vertical displacement at the quarter-span. The maximum displacement of 10 mm was defined in the displacement controlled quasi static analysis and it was ramped up during the analysis. The force on the beams was obtained from the reaction force of the beam. The mesh size of 20 mm was assigned to prestressing strands, rebar, shear links and end bearing plates. For the concrete beam, a mesh size of 20 mm was assigned to a region of 600 mm in length at the loading point while the rest of the beam was assigned with a coarser mesh of 30 mm to reduce computational time while maintaining the accuracy of FE analyses at the critical zone. Fig. 5 illustrates the mesh discretization of the post-tension concrete beams. Three mesh sizes were considered for mesh sensitivity study, namely 20 mm, 30 mm and 40 mm. Two criterion evaluated were the maximum load and the corresponding displacement. It was found that the maximum load variation was very small, it was 210.5 kN, 208.6 kN and 210.2 kN for 20 mm, 30 mm and 40 mm mesh, respectively. For the maximum displacement, it was 4.44 mm, 4.4 mm and 5.62 mm for 20 mm, 30 mm and 40 mm mesh, respectively. From these results, it showed that mesh sizes of 20 mm and 30 mm were adequate and 20 mm mesh was chosen because the plastic strain distribution predicted at the loaded quarter span was more refined.

Interaction between concrete with strands, rebar and shear links was modelled using the embedded constraint without bond-slip behavior. For the interaction between concrete at the interfaces, three contact algorithms evaluated were tie constraint, surface-based cohesive contact and surface-to-surface contact. The tie constraint assumes perfect bonding at the interface ignoring bond-slip. The surface-based cohesive contact could be used to model the bonding failure behavior of concrete and it is defined by the traction-separation constitutive model. However, this contact algorithm does not incorporate the friction interaction between the surfaces once the bonding failed. This constitutive model considers phenomena of linear elastic traction-separation, damage initiation criteria and damage evolution laws. The elastic stiffness at the concrete interfaces was based on underlying concrete elements stiffness. The shear damage initiation criteria and damage evolution were defined in accordance to Model code 2010. The shear damage initiation criteria used in this study was based on the maximum nominal stress. The resistance of the contact surface reduced once the shear stress reached the specified maximum shear stress. The maximum shear stress is in the range of 1.5 to 2.5 MPa for rough surface while it is 2.5 to 3.5 MPa for very rough surface (fib 2013). For the damage evolution, linear displacement softening was chosen with a maximum displacement of 0.05 mm.

For the surface-to-surface contact, it simulates friction interaction between surfaces. Kim *et al* (2014) used this contact algorithm to simulate interaction between tendons and sheathing of post-tensioned slabs with unbonded tendons. The chemical bonding was ignored in this contact algorithm, the shear transfer at the interface depended on the friction interaction and dowel action of stirrups for the concrete composite beams. The hard contact was defined in the normal direction, while the friction coefficient of 0.5 was defined in the tangential direction.

4.2 Material models

In this study, the concrete damage plasticity (CDP) model was used to model concrete behavior because this material model is suitable for plain and reinforced concrete structures with low confining pressure subjected to monotonic, cyclic and dynamic loading conditions. This model could also simulate the response of prestressed concrete structures (Ren *et al*. 2015). It considers cracking and crushing of concrete by non-associated multi-hardening plasticity in tension and compression. The non-associated potential plastic flow is modelled using the Drucker-Prager hyperbolic function considering parameters such as dilation angle (ψ) and flow potential eccentricity (ε) (Dassault

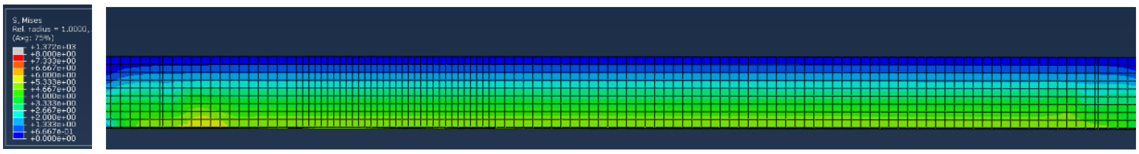

(a) stress distribution of the bottom concrete layer at the end of step 1

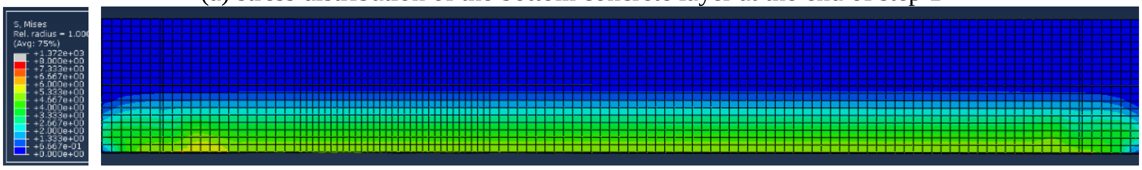

(b) activation of top layer of concrete

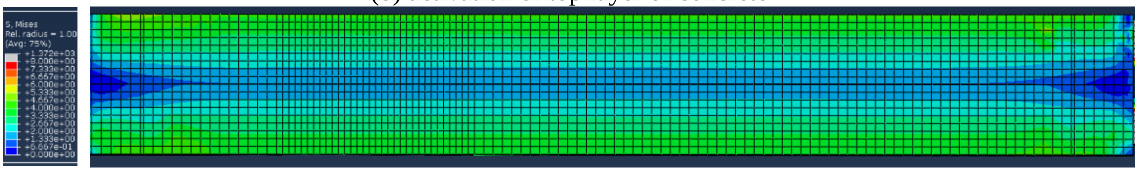

(c) stress distribution after activation of top strand

Fig. 6 Analysis sequence of 2C2S beam

Systemes 2016). Dilation angle may affect the shear resistance of concrete structures and a wide range of dilation angle, from 5^{o} (Wosatko *et al*. 2015) to 40^{o} (Navarro *et al*. 2018) has been adopted to simulate shear behaviour of reinforced concrete structures. It was found that reducing dilation angle resulted in a lower ultimate load. A typical value of 31^{o} was adopted in this study. The ratio of initial equibiaxial compressive yield stress to initial uniaxial compressive yield stress (f_{bo}/f_{co}) and the ratio of the second stress invariant on the tensile meridian to the compressive meridian (K_c) control the hardening response in tension and compression. Nominal values of damage plasticity parameters were adopted in this study as shown in Table 3. It is worth noting that the viscosity parameter may improve convergence rate in the softening region of concrete, however, it could lead to overestimation of maximum load. A viscosity parameter of 1×10^{-5} or less is normally chosen to improve the convergence rate while maintaining the accuracy of FE models.

The average concrete compressive strength at the day of beams testing was determined as 35.06 MPa. The tensile strength, elastic modulus and stress-strain relationship of concrete were determined based on the average concrete compressive strength in accordance to Model code 2010. The tensile strength was determined as 3.21 MPa. The stress-strain relationship in compression was defined as

$$\frac{\sigma_c}{f_{cm}} = -\left(\frac{k\eta-\eta^2}{1+(k-2)\eta}\right) \quad for\,|\varepsilon_c|\langle|\varepsilon_{c,\lim}| \qquad (1)$$
$$\eta = \varepsilon_c/\varepsilon_{c1} \qquad k = E_{ci}/E_{c1}$$

where $\varepsilon_{c,1}$ is the strain at the maximum compressive stress, $E_{c,1}$ is the secant modulus and k is the plasticity number. The tension stiffening behavior after concrete cracking was defined by the stress-cracking opening linear relationship determined based on the fracture energy (GF) of concrete to overcome the mesh dependency problem (Abdelatif *et al*. 2015).

Steel reinforcement was assumed as an elasto-plastic material where the yield stress of flexural rebar was 520 MPa while it was 250 MPa for stirrups. The behavior of prestressing strands was simplified into bilinear hardening relationship with the yield stress of 1674 MPa and the ultimate tensile strength of 1861 MPa. The Young's modulus for rebar and strands was 200 GPa and 195 GPa, respectively. The end bearing plates were assigned with elastic material properties with the Young's modulus of 200 GPa as no damage was observed after the tests.

4.3 Modelling of construction sequence of post-tensioned concrete composite beams

The geometry of concrete layer was defined according to the height of concrete in each casting. For instance, the concrete beam was modelled as a single part with a height of 450 mm for the control beam, while the 3C2S beam was divided into three parts with each part having a height of 150 mm. Multi-step analyses were defined in Abaqus/Standard to correctly capture the casting and stressing sequence of post-tensioned concrete beams. For the control beam, a two-step analysis was defined. In the first step, the prestressing stress was applied to the strands using prestress hold command. The stress was distributed from the strands to concrete and end bearing plates to achieve stress equilibrium at the end of first step. In the second step, the beam was loaded to failure. The same analysis sequence was applied to the 2C1S beam as the stressing sequence was the same, except two layers of concrete were modelled instead of a single part in the control beam. The number of analysis step increased for 2C2S and 3C2S beams due to the staged stressing. For the 2C2S and 3C2S beams, the same analysis sequence was defined as there were two stressing stages. In both beams, the bottom layer of concrete was stressed before casting of the next layer of concrete. The second stressing was performed after the last layer of concrete achieved sufficient strength. The model change interaction was used to deactivate and reactivate relevant parts to simulate removal or addition of parts in the model during analysis. In the first step, the bottom layer of concrete, bottom strand and relevant end bearing plates were activated and the stress was transferred from the bottom strand to concrete and end bearing plates to achieve stress equilibrium at the end of this step as shown in Fig. 6(a).

In the next step, the top layer of concrete was activated in the case of 2C2S beam, while the second and third layers of concrete were activated simultaneously for 3C2S beam. It could be observed that no stress was transferred from the bottom layer of concrete to the next layer as shown in Fig. 6(b). In the third step, the top strand was activated and the stress was transferred to the whole beam as shown in Fig. 6(c). In the final step, the beam was loaded to failure. For the beams with staged casting, tied constraint was used during simulation of concrete casting and staged stressing to ensure proper stress transfer between concrete layers. At the final analysis step where the beams were loaded to failure, the tied constraint was deactivated and cohesive contact or surface-to-surface contact was activated to evaluate effects of different contact algorithm on the beams response.

5. Evaluation of different contact interactions in finite element analysis

The predicted load-displacement responses were compared to the experimental results in Fig. 3. For the control beam, the FE model predicted a higher flexural stiffness and the stiffness started to reduce when the load reached 140 kN due to concrete cracking. The predicted plastic strain distribution agreed well with the experimental observation where flexural and flexural shear cracks could be observed as shown Fig. 7(a). The FE model predicted the maximum load of 210.8 kN, which was about 5% lower than the experimental maximum load as shown in Table 2. The FE model predicted concrete crushing and yielding of the tensile reinforcements at the maximum load. Overall, the FE model could predict the maximum load of control beams accurately.

Three types of contact evaluated for beams with staged construction were tie constraint, cohesive contact and surface-to-surface contact. The maximum shear strength for cohesive contact and the friction coefficient for surface-to-surface contact were determined based on the FE model calibrations. The maximum shear strength of 3.5 MPa was chosen for cohesive contact, while the friction coefficient was 0.5. Adopting lower shear strength or coefficient of friction resulted in significantly underestimating the flexural capacity of beams. When tie constraint was defined at the interface, the predicted maximum load was 208.7 kN, 203.8 kN and 210.5 kN for 2C1S, 2C2S and 3C2S, respectively. These values were close to the maximum load predicted by the control beam of 210.8 kN, with a maximum difference of 4%. The small variations of maximum load could be due to the approximation of numerical method employed in the analysis. These results indicated that the FE models using tie constraint predicted monolithic behavior for beams with staged casting. Tie constraint is not recommended as it could not simulate the effects of interface slip on the maximum load of concrete composite beams.

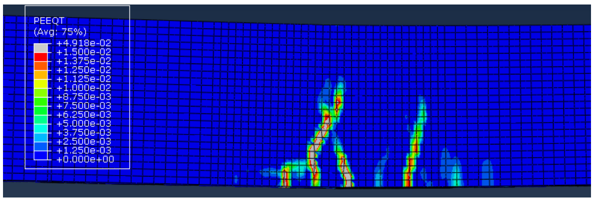

(a) control beam

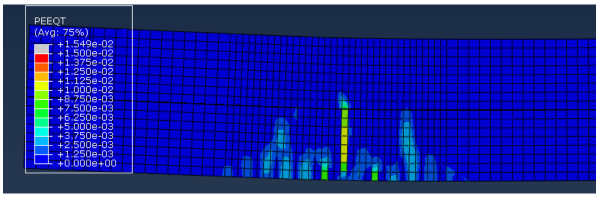

(b) 2C1S beam using cohesive contact

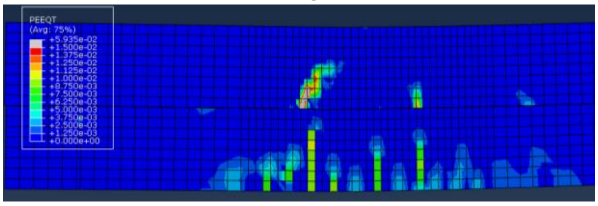

(c) 2C1S beam using surface-to-surface contact

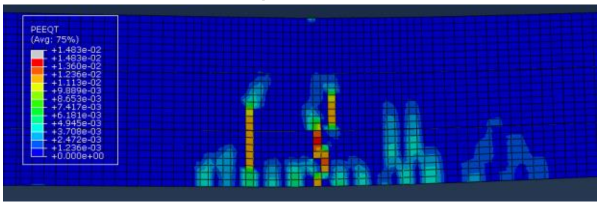

(d) 3C2S beam using cohesive contact

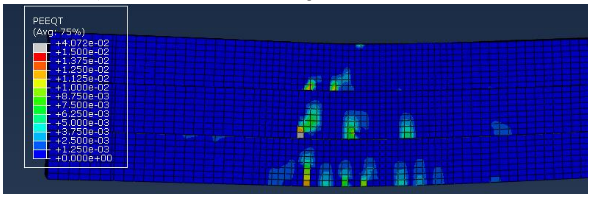

(e) 3C2S beam using surface-to-surface contact.

Fig. 7 Plastic strain distribution predicted by FE models

The predicted response of FE models using cohesive contact was similar to the corresponding FE model with tie constraint except the maximum load was reduced as shown in Fig. 3 (b) to (d). It could be observed that both tie constraint and cohesive contact predicted higher initial stiffness compared to the experimental results for all the beams. The possible reason for this discrepancy was low initial stiffness recorded in the experiments. The low initial stiffness could be due to small gaps between the supports and beams. Once, the gaps were eliminated by the applied load, the stiffness became constant up to crack initiation.

The failure of cohesive contact resulted in a lower maximum load, about 10% compared to the results of FE models using tie constraint. The tensile reinforcement was not yielded at the maximum load for all the beams due to interface slip. The maximum loads predicted by FE models using cohesive contact were lower than the experimental results, with a maximum difference of 14% as summarized in Table 2. The plastic strain distribution of FE models using cohesive contact for 2C1S and 3C2S beams is

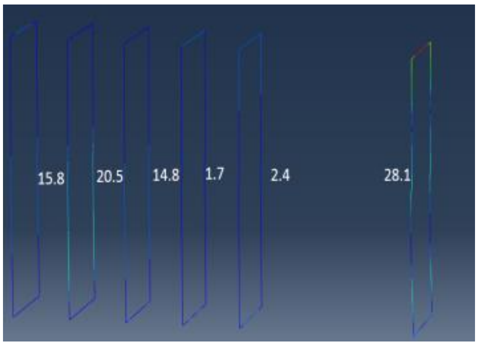

(a) 2C2S beam using cohesive contact

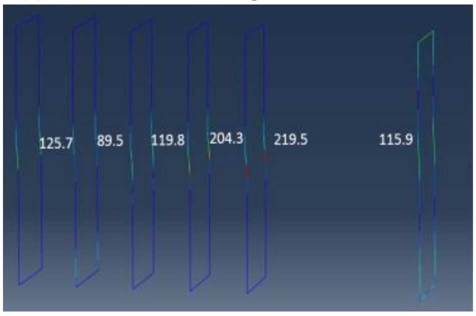

(b) 2C2S beam using surface-to-surface contact

Fig. 8 Von Mises stress contour plots of shear links (the values show stresses at the concrete interface, unit: MPa)

illustrated in Fig. 7 (b) and (d). The predicted plastic strain distribution of 2C2S beam was similar to 2C1S beam illustrated in Fig. 7(b). It could be observed that the FE models were able to accurately simulate the increased number of cracks for beams with staged construction compared to the control beam by comparing Fig. 7 (a), (b) and (d). Fig. 8(a) shows that shear links experienced low stress, less than 30 MPa, due to the slip at the concrete interface at the maximum load. The first shear link adjacent to the loaded quarter span experienced highest stress (28.1 MPa) indicating that the largest slip occurred near the loading point. It is worth noting that the simulation was terminated due to convergence issue in the cohesive contact, and this may not model the physical interactions such as friction between surfaces and dowel action which is important for heavily reinforced composite beam across the interface. Further research is required to evaluate the effectiveness of cohesive contact for concrete composite beams with different ratio of stirrups.

The FE models using surface-to-surface contact with a friction coefficient of 0.5 underestimated flexural stiffness of beams with staged construction due to omission of composite action. By comparing the predicted stiffness of 2C1S and 3C1S beams, it could be observed that the stiffness reduced as the number of concrete casting increased. The cracks initiated at the soffit of each layer and propagated upward as shown in Fig. 7 (c) and (e). The interface shear force was transferred by friction interaction and dowel action of shear links. The shear links were subjected to higher stress concentration at the concrete interface compared to the model using cohesive contact due to the slip between different layers as demonstrated in Fig. 8(b). The highest stress of 219.5 MPa was recorded at the second shear link adjacent to the loaded quarter span indicating that the maximum slip occurred at a certain distance from the loading point.The maximum load predicted for beams with two casting (2C1S and 2C2S) was about 10% lower than the experimental results as shown in Table 2.

However, the predicted maximum load for 3C2S beam was more conservative, about 25% lower than the experimental maximum load. For the beam with two concrete layers, interface slip was observed in the experiments before the beams reached the maximum load. Therefore the FE models using surface-to-surface contact modelled the response of 2C1S and 2C2S beams correctly at the ultimate limit state. While interface slip could only be observed at the interface between the bottom and middle layers of 3C2S beams in the experiments.

The omission of chemical bonding between the middle to top concrete layers resulted in much lower maximum load in the FE analysis. The beams failed by concrete crushing at the loading point while the flexural reinforcement remained elastic. From these results, it could be deduced that surface-to-surface contact could be used to predict the maximum load of concrete composite beams with two casting as it is expected that the interface slip occurred before the beams reached the maximum load. The use of this contact algorithm is not recommended for beams with more than two layers of concrete as it underestimated the maximum load.

6. Conclusions

In this study, the static behavior of prestressed concrete composite beams with different casting and stressing sequence was investigated. The parameters investigated experimentally were the number of concrete casting and stressing sequence. The finite element models developed could accurately predict initial stress distribution in the composite beams induced by different casting and stressing sequence. Three contact algorithms namely tie constraint, cohesive contact and surface-to-surface contact were employed in the finite element analyses to simulate the interaction between concrete layers. Based on the results of this study, the following conclusions were drawn.

- The prestressed concrete composite beams could not achieve monolith behavior under three-point bending due to interface slip. The maximum load is governed by the interface shear strength and the initial stress distribution due to staged construction has little effect on the maximum load capacity.
- Staged construction affected crack distribution where cracks tend to propagate along the interface causing the failure of concrete bonding at the interface. For beams with three layers of concrete, cracks propagated along the bottom interface, while very minor cracking could be observed along the upper interface.
- From FE analyses, it was found that cohesive contact and surface-to-surface contact could be used to simulate the interface slip of concrete composite beams even though each contact considers different shear transfer mechanism. The cohesive contact simulates the concrete

adhesion while surface-to-surface contact considers friction interaction and dowel action from shear links. The surface-to-surface contact ignores the chemical bonding of concrete therefore underestimates the flexural stiffness of concrete composite beams. The use of surface-to-surface contact for beams with more than two concrete castings is not recommended as it may underestimate the maximum load.

Further research is recommended to investigate the capability of cohesive contact in analyzing the maximum load of concrete composite beams with different ratio of shear reinforcement at the interface.

Acknowledgments

This work was undertaken with funding from OSD Consultant Sdn Bhd and Nehemiah Prestress Sdn Bhd. The authors would like to express their gratitude to Ir Chang Chee Cheong (BBR Malaysia) for sponsoring the prestressing systems and Mr Dominic Hoy for his kind assistance in samples preparation and testing. Technical supports provided by Dr Neha Parool from Advisian Singapore for the Abaqus modelling is greatly appreciated.

References

Abdelatif, A.O., Owen, J.S. and Hussein, M.F.M. (2015), "Modelling the prestress transfer in pre-tensioned concrete elements", *Finite Elem. Anal. Des.*, **94**, 47-63. https://doi.org/10.1016/j.finel.2014.09.007.

Adawi, A., Youssef, M.A. and Meshaly, M.E. (2015), "Experimental investigation of the composite action between hollowcore slabs with machine-cast finish and concrete topping", *Eng. Struct.*, **91**, 1-15. https://doi.org/10.1016/j.engstruct.2015.02.018.

Adawi, A., Youssef, M.A. and Meshaly, M.E. (2016), "Finite element modeling of the composite action between hollowcore slabs and the topping concrete", *Eng. Struct.*, **124**, 302-315. https://doi.org/10.1016/j.engstruct.2016.06.016.

Baran, E. (2015), "Effects of cast-in-place concrete topping on flexural response of precast concrete hollow-core slabs", *Eng. Struct.*, **98**, 109-117. https://doi.org/10.1016/j.engstruct.2015.04.017.

Costa, H., Carmo, R.N.F. and Júlio, E. (2018), "Influence of lightweight aggregates concrete on the bond strength of concrete-to-concrete interfaces", *Constr. Build. Mater.*, **180**, 519-530. https://doi.org/10.1016/j.conbuildmat.2018.06.011.

Dassault Systemes (2016), Abaqus User Manual.

Dias-da-Costa, D., Alfaiate, J. and Júlio, E.N.B.S. (2012), "FE modeling of the interfacial behaviour of composite concrete members", *Constr. Build. Mater.*, **26**(1), 233-243. https://doi.org/10.1016/j.conbuildmat.2011.06.015.

Fang, Z., Jiang, H., Liu, A., Feng, J. and Chen Y. (2018), "Horizontal shear behaviors of normal weight and lightweight concrete composite T-beams", *Int. J. Concrete Struct. Mater.*, **12**(1), 55. https://doi.org/10.1186/s40069-018-0274-3.

Fernandes, H., Lúcio, V. and Ramos, A. (2017), "Strengthening of RC slabs with reinforced concrete overlay on the tensile face", *Eng. Struct.*, **132**, 540-550. https://doi.org/10.1016/j.engstruct.2016.10.011.

fib (2013), fib Model Code for Concrete Structures 2010, fédération internationale du béton.

Halicka, A. (2011), "Influence new-to-old concrete interface qualities on the behaviour of support zones of composite concrete beams", *Constr. Build. Mater.*, **25**(10), 4072-4078. https://doi.org/10.1016/j.conbuildmat.2011.04.045.

He, Y., Zhang, X., Hooton, R.D. and Zhang, X. (2017), "Effects of interface roughness and interface adhesion on new-to-old concrete bonding", *Constr. Build. Mater.*, **151**, 582-590. https://doi.org/10.1016/j.conbuildmat.2017.05.049.

Jiang, H., Fang, Z., Liu, A., Li, Y. and Feng, J. (2016), "Interface shear behavior between high-strength precast girders and lightweight cast-in-place slabs", *Constr. Build. Mater.*, **128**, 449-460. https://doi.org/10.1016/j.conbuildmat.2016.10.088.

Júlio, E.N.B.S., Dias-da-Costa, D., Branco, F.A.B. and Alfaiate, J.M.V. (2010), "Accuracy of design code expressions for estimating longitudinal shear strength of strengthening concrete overlays", *Eng. Struct.*, **32**(8), 2387-2393. https://doi.org/10.1016/j.engstruct.2010.04.013.

Kim, J.R. and Kwak, H.G. (2018), "FE analyses and prediction of bursting forces in post-tensioned anchorage zone", *Comput. Concrete*, **21**(1), 75-85. https://doi.org/10.12989/cac.2018.21.1.075.

Kim, U., Huang, Y., Chakrabarti, P.R. and Kang, T.H.K. (2014), "Modeling of post-tensioned one-way and two-way slabs with unbonded tendons", *Comput. Concrete*, **13**(5), 587-601. https://doi.org/10.12989/cac.2014.13.5.587.

Kwak, H.G. and Hwang, J.W. (2010), "FE model to simulate bond-slip behavior in composite concrete beam bridges", *Comput. Struct.*, **88**(17), 973-984. https://doi.org/10.1016/j.compstruc.2010.05.005.

Kwak, H.G., Kim, J.H. and Kim, S.H. (2006), "Nonlinear analysis of prestressed concrete structures considering slip behavior of tendons", *Comput. Concrete*, **3**(1), 43-64. http://dx.doi.org/10.12989/cac.2006.3.1.043.

Lesley, H., Sneed, K.K., Samantha, W. and Donald, M. (2016), "Interface shear transfer of lightweight-aggregate concretes with different lightweight aggregates", *PCI J.*, **61**(2), 38-55.

Loov, R.E. and Patnaik, A.K. (1994), "Horizontal shear strength of composite concrete beams with a rough interface", *PCI J.*, **39**(1), 48-69.

Mohamad, M.E., Ibrahim, I.S., Abdullah, R., Rahman, A.B., Abd., Kueh, A.B.H. and Usman, J. (2015), "Friction and cohesion coefficients of composite concrete-to-concrete bond", *Cement Concrete Compos.*, **56**, 1-14. https://doi.org/10.1016/j.cemconcomp.2014.10.003.

Mones, R.M. and Breña, S.F. (2013), "Hollow-core slabs with cast-in-place concrete toppings: A study of interfacial shear strength", *PCI J.*, **58**(3), 124-141.

Navarro, M., Ivorra, S. and Varona, F.B. (2018), "Parametric computational analysis for punching shear in RC slabs", *Eng. Struct.*, **165**, 254-263. https://doi.org/10.1016/j.engstruct.2018.03.035.

Patnaik, A.K. (2001), "Behavior of composite concrete beams with smooth interface", *J. Struct. Eng.*, **127**(4), 359-366. https://doi.org/10.1061/(ASCE)0733-9445(2001)127:4(359).

Ren, W., Sneed, L.H., Yang, Y. and He, R. (2015), "Numerical simulation of prestressed precast concrete bridge deck panels using damage plasticity model", *Int. J. Concrete Struct. Mater.*, **9**(1), 45-54. https://doi.org/10.1007/s40069-014-0091-2.

Seible, F. and Latham, C.T. (1990), "Horizontal load transfer in structural concrete bridge deck overlays", *J. Struct. Eng.*, **116**(10), 2691-2710. https://doi.org/10.1061/(ASCE)0733-9445(1990)116:10(2691).

Standardization, E.C.F. (2005), Eurocode 2: Design of Concrete Structures.

Tsioulou, O.T., Lampropoulos, A.P. and Dritsos, S.E. (2013), "Experimental investigation of interface behaviour of RC beams strengthened with concrete layers", *Constr. Build. Mater.*, **40**, 50-59. https://doi.org/10.1016/j.conbuildmat.2012.09.093.

Wosatko, A., Pamin, J. and Polak M.A. (2015), "Application of damage–plasticity models in finite element analysis of punching shear", *Comput. Struct.*, **151**, 73-85. https://doi.org/10.1016/j.compstruc.2015.01.008.

Yin, H., Teo, W. and Shirai, K. (2017), "Experimental investigation on the behaviour of reinforced concrete slabs strengthened with ultra-high performance concrete", *Constr. Build. Mater.*, **155**, 463-474. https://doi.org/10.1016/j.conbuildmat.2017.08.077.

CC